Viscoelastically coupled in-plane and transverse dynamics of imperfect microplates

Mergen H. Ghayesh [a,*], Hamed Farokhi [b], Ali Farajpour [a]

[a] *School of Mechanical Engineering, University of Adelaide, South Australia 5005, Australia*
[b] *Department of Mechanical and Construction Engineering, Northumbria University, Newcastle upon Tyne NE1 8ST, UK*

**Corresponding author: mergen.ghayesh@adelaide.edu.au*
hamed.farokhi@northumbria.ac.uk (H Farokhi)
ali.farajpourouderji@adelaide.edu.au (A Farajpour)

Abstract

A Kelvin-Voigt based constitutive equation is implemented in Hamilton's framework in order to derive the coupled in-plane/transverse equations governing the motion of a microplate with geometric imperfections, while considering geometric nonlinearities. The Kirchhoff plate theory and the modified couple stress-based theory (MCST) are utilized to obtain the strain and kinetic energies of the imperfect microsystem. Then, the Kelvin–Voigt energy dissipation scheme is employed to derive expressions for the work of the viscous components of the classical and non-classical stress tensors. Frequency-response diagrams are plotted to investigate the nonlinear resonant oscillations of the imperfect viscoelastic microsystem in the presence of geometric imperfections. Numerical simulations revealed that the concurrent presence of geometric imperfections and the nonlinear amplitude-dependent damping mechanism alters the bifurcational behaviour of the viscoelastic microsystem substantially. It is shown that at oscillations of large amplitude, the nonlinear damping contributions become significant.

Keywords: *viscoelastic material; nonlinear dynamics; imperfect microscale plates; Kelvin–Voigt viscoelastic damping*; *modified couple stress theory* (MCST)

1. Introduction

Microresonators, microactuators, microswitches and biosensors are only a few examples of microelectromechanical systems (MEMS) where the core elements are microbeams and/or microplates [1-10]. Experimental investigations revealed that these microstructures display size-dependent behaviours associated with a small size, which can dramatically alter the resulting dynamics [11-13]. Many higher-order continuum models, such as the modified couple stress theory (MCST) [14-16], have been developed and applied to improve our understanding of the static and dynamical behaviour of these microsystems. Viscosity plays an important role in the mechanical behaviour of different systems; there are two conditions that make these effect dominant, namely the material itself is highly viscous such as polycarbonate and rubbers (which exhibit time-dependent stress-strain correlation) or when the operation temperature is relatively high [17]. In both the cases, a more general theory such as viscoelasticity is required to describe the mechanical properties of the materials. Additionally, it is shown that microdevices such as microresonators exhibit nonlinear damping [18] which results in a nonlinear amplitude-dependent damping response; this cannot be predicted, but through use of a nonlinear *viscoelastic* model.

In reality, microstructures, when manufactured, may not be perfectly flat due to improper processes; however, in some applications, they are made with initial curvature intentionally. Therefore, an extensive coupled nonlinear size-dependent model accounting for

the viscoelasticity of the material as well as initial imperfections is required to explore the effects of nonlinear amplitude-dependent damping and the imperfection amplitude on the vibrational response of microplates.

Compared to microscale and nanoscale structures with applications in small-scale devices such as nano-oscillators [19], the buckling, bending and vibration of macroscale structures have been extensively investigated in the literature. For instance, Zhang et al. [20] examined the nonlinear dynamic response of cylindrical shells made of functionally graded (FG) material via a shear deformation shell theory. Hao et al. [21] performed a thorough nonlinear analysis on the oscillations of cantilever FG plates using a perturbation method as well as a third-order theory of plates. Zhang et al. [22] also analysed the chaotic response of orthotropic plates made of FG material employing a plate model with shear deformations. In addition, Hao et al. [23] studied the large-amplitude vibration, bifurcation and chaotic behaviour of FG plates utilising Reddy's plate theory. Mahmoodi et al. [24] developed an analytical procedure to analyse the large-amplitude vibration of viscoelastic beams by employing a technique of multiple scales

The vibration, stability and deformation of microscale and nanoscale structures have also been studied via developing scale-dependent formulations. Lei et al. [25] explored the vibration of viscoelastic nanobeams using the Kelvin–Voigt model and a nonlocal model. In another investigation, Namvar et al. [26] conducted both experiments and theoretical analysis on the vibration response of U-shape microscopes using a couple stress model. Rahmani et al. [27] examined the vibration of curved nanobeams made of FG material incorporating couple

stress effects. In another study performed by Sourki and Hosseini [28], the effects of couple stress, nonlocal and surface energy were analysed on the vibrations of weakened beams at nanoscales. Zarepour and Hosseini [29] also presented a semi analytical approach for the large-amplitude vibrations of nanobeams subject to electro-thermo-mechanical loading.

To the authors' best of knowledge, no existing investigation in the literature has addressed the size-dependent forced *nonlinear dynamics of initially imperfect viscoelastic* microplates taking into account the coupled in-plane and transverse motions. The relevant literature on the *elastic* models of microplates is reviewed in the following. *Linear* and *nonlinear* studies are the two classes of studies in this context. Starting with the review of the first category (i.e. *linear* studies), Hashemi and Samaei [30] conducted a linear buckling analysis on nono/microplates under in-plane external loads employing the Mindlin nonlocal plate theory. Jomehzadeh et al. [31] employed MCST to obtain a linear model for the out-of-plane motion of a microplate and performed a vibration analysis. Further examinations were conducted by Wang et al. [32], who made use of a linear model, based on the Kirchhoff theory together with the strain gradient elasticity theory, to examine the size-dependent characteristics of microplates. In another study, Roque et al. [33] investigated the static behaviour of a shear deformable microplate using MSCT. Nabian et al. [34] conducted a stability analysis on the forced vibration response of a functionally graded (FG) micro-scale plate under electrostatic and hydrostatic loads. Ashoori et al. [35] utilised the modified strain-gradient theory to obtain the linear equation for the transverse motion of a microplate. The linear buckling behaviour of a sheet made of orthotropic graphene was studied by Farajpour et al. [36] using the nonlocal Eringen theory. Li et al. [37] made use of MCST to analyse the static response of a bi-layered

Kirchhoff microplate with simply supported boundary conditions. In contrast to the first category, i.e. the linear models, only a few studies in the literature were concerned with *geometric nonlinearities* in the mechanics of microplates. For instance, the equations governing the motion of a microplate were derived by Asghari [38] based on MCST. In another study, Thai and Choi [39] derived a model of FG Mindlin and Kirchhoff plates using MSCT.

As mentioned above, all the studies in the literature investigated the linear or nonlinear vibrations/bending of *perfectly flat* microplates on the basis of *elastic* models. The aim of this paper is to explore the *forced nonlinear oscillations of an imperfect viscoelastic microplate* by means of MCST; this is for the first time. The imperfect viscoelastic microplate is modelled employing the Kirchhoff plate theory considering the von Kármán nonlinearities as well as MCST for the small-size effects. A general distribution of imperfection is considered in the transverse component of the displacement field. The Kelvin–Voigt viscoelastic scheme is utilised to derive the expressions for the nonlinear damping in the presence of geometric nonlinearities. All the transverse and in-plane terms in inertia and displacement are retained in both modelling and simulations; extensive numerical simulations are performed to examine the effect of the presence of geometric imperfections, the contribution of the amplitude-dependent nonlinear damping terms, and the significance of considering the small size of the microplate on the nonlinear dynamics.

2. Continuous model development

An imperfect viscoelastic microplate of thickness *h*, dimensions *a* and *b*, Young's and shear moduli *E* and μ, respectively, Poisson's ratio ν, and mass density ρ, is depicted in Fig. 1. A distributed harmonic force, $F_1\cos(\omega t)$, is exerted on the microplate in the positive *z* direction[40]; F_1 is the excitation amplitude per unit area in N/m^2, *t* is time, and ω denotes the excitation frequency in rad/s. The microplate is fully clamped at all edges; the motion is described in a Cartesian coordinate system. The microplate mid-plane displacements in the *z*, *x*, and *y* directions are shown by $w= w(x,y,t)$, $u= u(x,y,t)$, and $v= v(x,y,t)$, respectively. According to the Kirchhoff plate theory [40, 41], the displacement field (**u**) components for an arbitrary point positioned at a general distance *z* from the mid-surface, in the presence of initial geometric imperfections, are formulated as

$$\begin{Bmatrix} u_1 \\ u_2 \\ u_3 \end{Bmatrix} = \begin{Bmatrix} -z\,\partial w/\partial x + u \\ -z\,\partial w/\partial y + v \\ w_0 + w \end{Bmatrix}, \tag{1}$$

where $w_0=w_0(x,y)$ denotes the initial geometric imperfection.

2.1 Microsystem energies and the work of external load and Kelvin-Voigt damping

The potential strain energy of the microplate occupying volume Λ is formulated utilising the MCST [42], which in variational form is given by

$$\Pi = \int_{\Lambda}\left[(\delta\boldsymbol{\varepsilon}:\boldsymbol{\sigma}) + (\delta\boldsymbol{\chi}:\mathbf{m})\right]\mathrm{d}\Lambda, \tag{2}$$

where ε, σ, χ, and **m** denote respectively the strain, stress, symmetric rotation gradient, and deviatoric part of the symmetric couple-stress tensors.

The symmetric rotation gradient tensor can be formulated as a function of the rotation vector θ; the expressions for χ and θ are given by [43]

$$\boldsymbol{\chi} = \frac{1}{2}\left((\nabla\boldsymbol{\theta})^{\mathrm{T}} + \nabla\boldsymbol{\theta}\right), \qquad \boldsymbol{\theta} = \frac{1}{2}\nabla\times\mathbf{u}. \tag{3}$$

Hence, the components of χ (assuming zero initial stress condition) can be obtained as

$$\begin{aligned}
&\left\{\chi_{xx},\chi_{yy},\chi_{zz}\right\} = \left\{\frac{\partial^2 w}{\partial x\partial y}, -\frac{\partial^2 w}{\partial x\partial y}, 0\right\} \\
&\left\{\chi_{xy},\chi_{xz},\chi_{yz}\right\} = \frac{1}{2}\left\{\left(\frac{\partial^2 w}{\partial y^2} - \frac{\partial^2 w}{\partial x^2}\right), \frac{1}{2}\left(\frac{\partial^2 v}{\partial x^2} - \frac{\partial^2 u}{\partial x\partial y}\right), \frac{1}{2}\left(\frac{\partial^2 v}{\partial x\partial y} - \frac{\partial^2 u}{\partial y^2}\right)\right\}
\end{aligned} \tag{4}$$

The nonzero components of the strain tensor for a geometrically imperfect microplate, accounting for von-Kármán nonlinear strains, are given by

$$\begin{aligned}
\varepsilon_{xx} &= \left(\frac{\partial w}{\partial x}\right)\left[\frac{1}{2}\left(\frac{\partial w}{\partial x}\right) + \frac{\partial w_0}{\partial x}\right] + \frac{\partial u}{\partial x} - z\frac{\partial^2 w}{\partial x^2}, \\
\varepsilon_{yy} &= \left(\frac{\partial w}{\partial y}\right)\left[\frac{1}{2}\left(\frac{\partial w}{\partial y}\right) + \frac{\partial w_0}{\partial y}\right] + \frac{\partial v}{\partial y} - z\frac{\partial^2 w}{\partial y^2}, \\
\varepsilon_{xy} &= \frac{1}{2}\left[\left(\frac{\partial w}{\partial y}\frac{\partial w}{\partial x} + \frac{\partial w_0}{\partial x}\frac{\partial w}{\partial y} + \frac{\partial w_0}{\partial y}\frac{\partial w}{\partial x}\right) + \frac{\partial u}{\partial y} + \frac{\partial v}{\partial x} - 2z\frac{\partial^2 w}{\partial x\partial y}\right].
\end{aligned} \tag{5}$$

Based on the Kelvin–Voigt viscoelastic damping mechanism, the stress in the system consists of an elastic part as well as a viscous part. To differentiate between the two parts, subscripts “e”

and “vis” denote the elastic and viscous components of $\boldsymbol{\sigma}$ and **m**. Under plane-stress condition, the non-zero elastic and viscous components of $\boldsymbol{\sigma}$ can be written as

$$\left\{\sigma_{xx(e)},\sigma_{yy(e)},\sigma_{xy(e)}\right\}=\frac{E}{\left(1-\nu^2\right)}\left\{\left(\nu\varepsilon_{yy}+\varepsilon_{xx}\right),\left(\nu\varepsilon_{xx}+\varepsilon_{yy}\right),\left(1-\nu\right)\varepsilon_{xy}\right\}, \tag{6}$$

$$\left\{\sigma_{xx(vis)},\sigma_{yy(vis)},\sigma_{xy(vis)}\right\}=\frac{E}{\left(1-\nu^2\right)}\eta\frac{\partial}{\partial t}\left\{\left(\nu\varepsilon_{yy}+\varepsilon_{xx}\right),\left(\nu\varepsilon_{xx}+\varepsilon_{yy}\right),\left(1-\nu\right)\varepsilon_{xy}\right\}, \tag{7}$$

in which η stands for the material viscosity coefficient.

Based on MCST, the elastic and viscous components of **m** can be written as

$$m_{jk(e)}=\frac{1}{\left(1+\nu\right)}El^2\chi_{jk}, \tag{8}$$

$$m_{jk(vis)}=\frac{1}{\left(1+\nu\right)}El^2\eta\frac{\partial}{\partial t}\chi_{jk}, \tag{9}$$

where l denotes the characteristic length-scale of the material.

Introducing the following stress-resultants

$$\begin{aligned}\left\{N_{x(e)},N_{y(e)},N_{xy(e)}\right\}&=\int_{-\frac{h}{2}}^{\frac{h}{2}}\left\{\sigma_{xx(e)},\sigma_{yy(e)},\sigma_{xy(e)}\right\}\mathrm{d}z,\\ \left\{M_{x(e)},M_{y(e)},M_{xy(e)}\right\}&=\int_{-\frac{h}{2}}^{\frac{h}{2}}z\left\{\sigma_{xx(e)},\sigma_{yy(e)},\sigma_{xy(e)}\right\}\mathrm{d}z,\end{aligned} \tag{10}$$

$$\left\{NC_{x(e)},NC_{y(e)},NC_{xy(e)},NC_{xz(e)},NC_{yz(e)}\right\}=\int_{-\frac{h}{2}}^{\frac{h}{2}}\left\{m_{xx(e)},m_{yy(e)},m_{xy(e)},m_{xz(e)},m_{yz(e)}\right\}\mathrm{d}z, \tag{11}$$

the variation of the potential strain energy of the system can be written as

$$\delta\Pi = \int_0^a \int_0^b \Bigg[N_{x(e)} \left(\frac{\partial}{\partial x}\delta u + \left(\frac{\partial w_0}{\partial x} + \frac{\partial w}{\partial x} \right) \frac{\partial}{\partial x}\delta w \right) - M_{x(e)} \frac{\partial^2}{\partial x^2}\delta w$$
$$+ N_{y(e)} \left(\frac{\partial}{\partial y}\delta v + \left(\frac{\partial w_0}{\partial y} + \frac{\partial w}{\partial y} \right) \frac{\partial}{\partial y}\delta w \right) - M_{y(e)} \frac{\partial^2}{\partial y^2}\delta w$$
$$+ N_{xy(e)} \left(\frac{\partial}{\partial x}\delta v + \frac{\partial}{\partial y}\delta u + \left(\frac{\partial w_0}{\partial y} + \frac{\partial w}{\partial y} \right) \frac{\partial}{\partial x}\delta w + \left(\frac{\partial w_0}{\partial x} + \frac{\partial w}{\partial x} \right) \frac{\partial}{\partial y}\delta w \right) \tag{12}$$
$$- 2M_{xy(e)} \frac{\partial^2}{\partial x \partial y}(\delta w) + NC_{x(e)} \frac{\partial^2}{\partial x \partial y}(\delta w) - NC_{y(e)} \frac{\partial^2}{\partial x \partial y}(\delta w) + NC_{xy(e)} \left(\frac{\partial^2}{\partial y^2}\delta w - \frac{\partial^2}{\partial x^2}\delta w \right)$$
$$- \frac{NC_{xz(e)}}{2} \left(\frac{\partial^2}{\partial x \partial y}\delta u - \frac{\partial^2}{\partial x^2}\delta v \right) - \frac{NC_{yz(e)}}{2} \left(\frac{\partial^2}{\partial y^2}\delta u - \frac{\partial^2}{\partial x \partial y}\delta v \right) \Bigg] \mathrm{d}y\mathrm{d}x,$$

The virtual work of the internal Kelvin-Voigt dissipation model can be formulated as

$$\delta W_{vis} = -\int_0^a \int_0^b \Bigg[N_{x(vis)} \left(\frac{\partial}{\partial x}\delta u + \left(\frac{\partial w_0}{\partial x} + \frac{\partial w}{\partial x} \right) \frac{\partial}{\partial x}\delta w \right) - M_{x(vis)} \frac{\partial^2}{\partial x^2}\delta w$$
$$+ N_{y(vis)} \left(\frac{\partial}{\partial y}\delta v + \left(\frac{\partial w_0}{\partial y} + \frac{\partial w}{\partial y} \right) \frac{\partial}{\partial y}\delta w \right) - M_{y(vis)} \frac{\partial^2}{\partial y^2}\delta w - 2M_{xy(vis)} \frac{\partial^2}{\partial x \partial y}\delta w$$
$$+ N_{xy(vis)} \left(\frac{\partial}{\partial y}\delta u + \frac{\partial}{\partial x}\delta v + \left(\frac{\partial w_0}{\partial y} + \frac{\partial w}{\partial y} \right) \frac{\partial}{\partial x}\delta w + \left(\frac{\partial w_0}{\partial x} + \frac{\partial w}{\partial x} \right) \frac{\partial}{\partial y}\delta w \right) \tag{13}$$
$$+ NC_{x(vis)} \frac{\partial^2}{\partial x \partial y}(\delta w) - NC_{y(vis)} \frac{\partial^2}{\partial x \partial y}(\delta w) + NC_{xy(vis)} \left(\frac{\partial^2}{\partial y^2}\delta w - \frac{\partial^2}{\partial x^2}\delta w \right)$$
$$+ \frac{NC_{xz(vis)}}{2} \left(\frac{\partial^2}{\partial x^2}\delta v - \frac{\partial^2}{\partial x \partial y}\delta u \right) + \frac{NC_{yz(vis)}}{2} \left(\frac{\partial^2}{\partial x \partial y}\delta v - \frac{\partial^2}{\partial y^2}\delta u \right) \Bigg] \mathrm{d}y\mathrm{d}x,$$

in which

$$\left\{ N_{x(vis)}, N_{y(vis)}, N_{xy(vis)} \right\} = \int_{-\frac{h}{2}}^{\frac{h}{2}} \left\{ \sigma_{xx(vis)}, \sigma_{yy(vis)}, \sigma_{xy(vis)} \right\} \mathrm{d}z,$$
$$\left\{ M_{x(vis)}, M_{y(vis)}, M_{xy(vis)} \right\} = \int_{-\frac{h}{2}}^{\frac{h}{2}} z \left\{ \sigma_{xx(vis)}, \sigma_{yy(vis)}, \sigma_{xy(vis)} \right\} \mathrm{d}z, \tag{14}$$

$$\left\{NC_{x(vis)}, NC_{y(vis)}, NC_{xy(vis)}, NC_{xz(vis)}, NC_{yz(vis)}\right\} = \int_{-\frac{h}{2}}^{\frac{h}{2}} \left\{m_{xx(vis)}, m_{yy(vis)}, m_{xy(vis)}, m_{xz(vis)}, m_{yz(vis)}\right\} \mathrm{d}z. \tag{15}$$

The variation of the kinetic energy of the imperfect viscoelastic microplate is formulated as

$$\delta T = \rho \int_0^a \int_0^b \int_{-\frac{h}{2}}^{\frac{h}{2}} \left[\left(\frac{\partial}{\partial t} \delta w \right) \frac{\partial w}{\partial t} + \left(\frac{\partial}{\partial t} \delta v \right) \frac{\partial v}{\partial t} + \left(\frac{\partial}{\partial t} \delta u \right) \frac{\partial u}{\partial t} \right] \mathrm{d}z \mathrm{d}x \mathrm{d}y, \tag{16}$$

The virtual work of the external distributed dynamic load is expressed as

$$\delta W_{ext} = \int_0^a \int_0^b \delta w \left(F_1 \cos(\omega t) \right) \mathrm{d}y \, \mathrm{d}x. \tag{17}$$

2.2 Equations of motion

Using Hamilton's energy principle, the three viscoelastically coupled nonlinear partial differential equations of motion can be derived as

$$\rho h \frac{\partial^2 u}{\partial t^2} - \frac{\partial N_{xy}}{\partial y} - \frac{\partial N_x}{\partial x} - \frac{1}{2} \frac{\partial}{\partial y} \left(\frac{\partial NC_{yz}}{\partial y} + \frac{\partial NC_{xz}}{\partial x} \right) = 0, \tag{18}$$

$$\rho h \frac{\partial^2 v}{\partial t^2} - \frac{\partial N_{xy}}{\partial x} - \frac{\partial N_y}{\partial y} + \frac{1}{2} \frac{\partial}{\partial x} \left(\frac{\partial NC_{yz}}{\partial y} + \frac{\partial NC_{xz}}{\partial x} \right) = 0, \tag{19}$$

$$\begin{aligned} &\rho h \frac{\partial^2 w}{\partial t^2} - \frac{\partial}{\partial x} \left[N_x \left(\frac{\partial w_0}{\partial x} + \frac{\partial w}{\partial x} \right) + N_{xy} \left(\frac{\partial w_0}{\partial y} + \frac{\partial w}{\partial y} \right) \right] - \left(\frac{\partial^2 M_x}{\partial x^2} + 2 \frac{\partial^2 M_{xy}}{\partial x \partial y} + \frac{\partial^2 M_y}{\partial y^2} \right) \\ &- \frac{\partial}{\partial y} \left[N_y \left(\frac{\partial w_0}{\partial y} + \frac{\partial w}{\partial y} \right) + N_{xy} \left(\frac{\partial w_0}{\partial x} + \frac{\partial w}{\partial x} \right) \right] \\ &- \frac{\partial}{\partial x} \left(\frac{\partial NC_{xy}}{\partial x} + \frac{\partial NC_y}{\partial y} \right) + \frac{\partial}{\partial y} \left(\frac{\partial NC_{xy}}{\partial y} + \frac{\partial NC_x}{\partial x} \right) - F_1 \cos(\omega t) = 0, \end{aligned} \tag{20}$$

in which

$$\begin{aligned}\left\{N_x, N_y, N_{xy}\right\} &= \left\{\left(N_{x(e)} + N_{x(vis)}\right), \left(N_{y(e)} + N_{y(vis)}\right), \left(N_{xy(e)} + N_{xy(vis)}\right)\right\}, \\ \left\{M_x, M_y, M_{xy}\right\} &= \left\{\left(M_{x(e)} + M_{x(vis)}\right), \left(M_{y(e)} + M_{y(vis)}\right), \left(M_{xy(e)} + M_{xy(vis)}\right)\right\},\end{aligned} \tag{21}$$

$$\begin{aligned}\left\{NC_x, NC_y, NC_{xy}, NC_{xz}, NC_{yz}\right\} = \left\{\left(NC_{x(e)} + NC_{x(vis)}\right), \left(NC_{y(e)} + NC_{y(vis)}\right), \left(NC_{xy(e)} + NC_{xy(vis)}\right)\right. \\ \left.\left(NC_{xz(e)} + NC_{xz(vis)}\right), \left(NC_{yz(e)} + NC_{yz(vis)}\right)\right\}.\end{aligned} \tag{22}$$

Substituting the resultant expressions of Eqs. (21) and (22) in Eqs. (18)-(20) gives the viscoelastically coupled nonlinear equations for the motion for the imperfect viscoelastic microplate in the in-plane and out-of-plane (transverse) directions as

$$\begin{aligned}&\rho h \frac{\partial^2 u}{\partial t^2} - \frac{Eh}{2(1+\nu)} \frac{\partial}{\partial y} \left\{ \left(1 + \eta \frac{\partial}{\partial t}\right) \left(\frac{\partial u}{\partial y} + \frac{\partial w_0}{\partial x} \frac{\partial w}{\partial y} + \frac{\partial v}{\partial x} + \frac{\partial w_0}{\partial y} \frac{\partial w}{\partial x} + \frac{\partial w}{\partial x} \frac{\partial w}{\partial y} \right) \right\} \\ &- \frac{Eh}{1-\nu^2} \frac{\partial}{\partial x} \left\{ \left(1 + \eta \frac{\partial}{\partial t}\right) \left[\left(\frac{1}{2} \left(\frac{\partial w}{\partial x} \right)^2 + \frac{\partial u}{\partial x} + \frac{\partial w_0}{\partial x} \frac{\partial w}{\partial x} \right) + \nu \left(\frac{1}{2} \left(\frac{\partial w}{\partial y} \right)^2 + \frac{\partial v}{\partial y} + \frac{\partial w_0}{\partial y} \frac{\partial w}{\partial y} \right) \right] \right\} \\ &- \frac{Ehl^2}{8(1+\nu)} \frac{\partial^2}{\partial y^2} \left[\left(1 + \eta \frac{\partial}{\partial t}\right) \left(\frac{\partial^2 v}{\partial x \partial y} - \frac{\partial^2 u}{\partial y^2} \right) \right] \\ &- \frac{Ehl^2}{8(1+\nu)} \frac{\partial^2}{\partial x \partial y} \left[\left(1 + \eta \frac{\partial}{\partial t}\right) \left(\frac{\partial^2 v}{\partial x^2} - \frac{\partial^2 u}{\partial x \partial y} \right) \right] = 0,\end{aligned} \tag{23}$$

$$\rho h\frac{\partial^2 v}{\partial t^2}-\frac{Eh}{2(1+\nu)}\frac{\partial}{\partial x}\left\{\left(1+\eta\frac{\partial}{\partial t}\right)\left(\frac{\partial u}{\partial y}+\frac{\partial w_0}{\partial x}\frac{\partial w}{\partial y}+\frac{\partial v}{\partial x}+\frac{\partial w_0}{\partial y}\frac{\partial w}{\partial x}+\frac{\partial w}{\partial y}\frac{\partial w}{\partial x}\right)\right\}$$
$$-\frac{Eh}{1-\nu^2}\frac{\partial}{\partial y}\left\{\left(1+\eta\frac{\partial}{\partial t}\right)\left[\left(\frac{1}{2}\left(\frac{\partial w}{\partial y}\right)^2+\frac{\partial v}{\partial y}+\frac{\partial w_0}{\partial y}\frac{\partial w}{\partial y}\right)+\nu\left(\frac{1}{2}\left(\frac{\partial w}{\partial x}\right)^2+\frac{\partial u}{\partial x}+\frac{\partial w_0}{\partial x}\frac{\partial w}{\partial x}\right)\right]\right\}$$
$$-\frac{Ehl^2}{8(1+\nu)}\frac{\partial^2}{\partial x\partial y}\left[\left(1+\eta\frac{\partial}{\partial t}\right)\left(\frac{\partial^2 u}{\partial y^2}-\frac{\partial^2 v}{\partial x\partial y}\right)\right]$$
$$-\frac{Ehl^2}{8(1+\nu)}\frac{\partial^2}{\partial x^2}\left[\left(1+\eta\frac{\partial}{\partial t}\right)\left(\frac{\partial^2 u}{\partial x\partial y}-\frac{\partial^2 v}{\partial x^2}\right)\right]=0, \tag{24}$$

$$\rho h\frac{\partial^2 w}{\partial t^2}-F_1\cos(\omega t)+\left(\frac{Eh^3}{12(1-\nu^2)}+\frac{Ehl^2}{2(1+\nu)}\right)\left\{\left(1+\eta\frac{\partial}{\partial t}\right)\left[\frac{\partial^4 w}{\partial x^4}+2\frac{\partial^4 w}{\partial x^2\partial y^2}+\frac{\partial^4 w}{\partial y^4}\right]\right\}$$
$$-\frac{Eh}{1-\nu^2}\frac{\partial}{\partial x}\left\{\left(\frac{\partial w}{\partial x}+\frac{\partial w_0}{\partial x}\right)\left(1+\eta\frac{\partial}{\partial t}\right)\left[\left(\frac{1}{2}\left(\frac{\partial w}{\partial x}\right)^2+\frac{\partial u}{\partial x}+\frac{\partial w_0}{\partial x}\frac{\partial w}{\partial x}\right)+\nu\left(\frac{1}{2}\left(\frac{\partial w}{\partial y}\right)^2+\frac{\partial v}{\partial y}+\frac{\partial w_0}{\partial y}\frac{\partial w}{\partial y}\right)\right]\right\}$$
$$-\frac{Eh}{1-\nu^2}\frac{\partial}{\partial y}\left\{\left(\frac{\partial w}{\partial y}+\frac{\partial w_0}{\partial y}\right)\left(1+\eta\frac{\partial}{\partial t}\right)\left[\left(\frac{1}{2}\left(\frac{\partial w}{\partial y}\right)^2+\frac{\partial v}{\partial y}+\frac{\partial w_0}{\partial y}\frac{\partial w}{\partial y}\right)+\nu\left(\frac{1}{2}\left(\frac{\partial w}{\partial x}\right)^2+\frac{\partial u}{\partial x}+\frac{\partial w_0}{\partial x}\frac{\partial w}{\partial x}\right)\right]\right\}$$
$$-\frac{Eh}{2(1+\nu)}\frac{\partial}{\partial y}\left\{\left(\frac{\partial w}{\partial x}+\frac{\partial w_0}{\partial x}\right)\left[\left(1+\eta\frac{\partial}{\partial t}\right)\left(\frac{\partial w_0}{\partial x}\frac{\partial w}{\partial y}+\frac{\partial u}{\partial y}+\frac{\partial w_0}{\partial y}\frac{\partial w}{\partial x}+\frac{\partial v}{\partial x}+\frac{\partial w}{\partial x}\frac{\partial w}{\partial y}\right)\right]\right\}$$
$$-\frac{Eh}{2(1+\nu)}\frac{\partial}{\partial x}\left\{\left(\frac{\partial w}{\partial y}+\frac{\partial w_0}{\partial y}\right)\left[\left(1+\eta\frac{\partial}{\partial t}\right)\left(\frac{\partial w_0}{\partial x}\frac{\partial w}{\partial y}+\frac{\partial u}{\partial y}+\frac{\partial w_0}{\partial y}\frac{\partial w}{\partial x}+\frac{\partial v}{\partial x}+\frac{\partial w}{\partial x}\frac{\partial w}{\partial y}\right)\right]\right\}=0. \tag{25}$$

2.3 Discretisation

The partial differential equations (PDEs) of motion given in Eqs. (23)-(25) are discretised into a set of ordinary differential equations (ODEs) of dimension *N* employing a two-dimensional Galerkin scheme. The following series expansions are utilised to approximate the displacements of the imperfect viscoelastic microplate

$$
\begin{aligned}
w(x,y,t) &= \sum_{i=1}^{M_3}\sum_{j=1}^{N_3}\Phi_i\left(\frac{x}{a}\right)\Phi_j\left(\frac{y}{b}\right)w_{i,j}(t) \\
u(x,y,t) &= \sum_{i=1}^{M_1}\sum_{j=1}^{N_1}\sin\left(\frac{i\pi x}{a}\right)\sin\left(\frac{j\pi y}{b}\right)u_{i,j}(t), \\
v(x,y,t) &= \sum_{i=1}^{M_2}\sum_{j=1}^{N_2}\sin\left(\frac{i\pi x}{a}\right)\sin\left(\frac{j\pi y}{b}\right)v_{i,j}(t),
\end{aligned}
\tag{26}
$$

where Φ_i and Φ_j denote the trial functions for the transverse motion of the microplate which satisfy the fully clamped boundary conditions; $w_{i,j}(t)$, $v_{i,j}(t)$ and $u_{i,j}(t)$, denote the unknown time-dependent generalised coordinates. The assumed trial functions satisfy the following boundary conditions for a fully clamped microplate

$$
\begin{aligned}
&v = u = w = 0, \qquad \partial w/\partial x = 0, \qquad \text{at } x = a, 0, \\
&v = u = w = 0, \qquad \partial w/\partial y = 0, \qquad \text{at } y = b, 0.
\end{aligned}
\tag{27}
$$

The formulation for Φ_i is given by

$$
\Phi_i\left(\frac{x}{a}\right) = \cosh\left(\frac{\psi_i x}{a}\right) - \cos\left(\frac{\psi_i x}{a}\right) - \lambda_i\left[\sinh\left(\frac{\psi_i x}{a}\right) - \sin\left(\frac{\psi_i x}{a}\right)\right] \tag{28}
$$

with $\lambda_i = \left(\cosh\psi_i - \cos\psi_i\right)/\left(\sinh\psi_i - \sin\psi_i\right)$ and ψ_i being the *i*th root of the frequency equation for a doubly clamped beam.

Substitution of the displacements defined in Eq. (26) into Eqs. (23)-(25) and application of the Galerkin scheme results in a set of discretised equations consisting of *N* nonlinear second-order ordinary differential equations (ODEs). The resultant set of ordinary differential equations can be written as

$$\int_0^b\int_0^a \Gamma_x(x,y)\sin\left(\frac{i\pi x}{a}\right)\sin\left(\frac{j\pi y}{b}\right)dxdy=0,$$
$$\int_0^b\int_0^a \Gamma_y(x,y)\sin\left(\frac{i\pi x}{a}\right)\sin\left(\frac{j\pi y}{b}\right)dxdy=0, \qquad (29)$$
$$\int_0^b\int_0^a \Gamma_z(x,y)\Phi_i\left(\frac{x}{a}\right)\Phi_j\left(\frac{y}{b}\right)dxdy=0,$$

where Γ_x, Γ_y and Γ_z are respectively the left-hand side of Eqs. (23), (24) and (25) in which Eq. (26) is implemented. Through application of a change of variables, this set is transformed into a new set consisting of nonlinear first-order ODEs of dimension 2*N*. The resultant set of equations is solved with the aid of a continuation scheme together with time-integration as well as eigenvalue method for linear parts; the natural frequencies and the resonant response of the imperfect viscoelastic microsystem are obtained. To ensure reliable results, 32 generalised coordinates are retained in the discretised model, i.e. a model with 32 degrees of freedom is considered. The unknown time-dependent generalised coordinates considered in this study are: $u_{2,1}$, $u_{4,1}$, $u_{2,3}$, $u_{6,1}$, $u_{4,3}$, $u_{2,5}$, $u_{8,1}$, $u_{6,3}$, $u_{4,5}$, $u_{2,7}$, $u_{10,1}$, $v_{1,2}$, $v_{1,4}$, $v_{3,2}$, $v_{1,6}$, $v_{3,4}$, $v_{5,2}$, $v_{1,8}$, $v_{3,6}$, $v_{5,4}$, $v_{7,2}$, $v_{1,10}$, $w_{1,1}$, $w_{1,3}$, $w_{3,1}$, $w_{1,5}$, $w_{5,1}$,$w_{3,3}$, $w_{3,5}$, $w_{5,3}$, $w_{1,7}$, and $w_{7,1}$.

3. Numerical results

In this section, the bifurcation behaviour of the imperfect viscoelastic microplate is examined for a microplate with the dimensions of h=3 μm, a=500 μm, and b=500 μm; the material properties of the microplate are: E =69 GPa, ρ =2700 kg/m^3, and ν =0.33. The

fundamental transverse mode with the amplitude of A_0 is selected for the imperfection function. The following dimensionless quantities are introduced for this section

$$A^*_0 = \frac{A_0}{h}, \left(w,u,v\right)^* = \frac{\left(w,u,v\right)}{h}, x^* = \frac{x}{a}, y^* = \frac{y}{b},$$
$$f_1 = \frac{F_1 a^4}{Dh}, t^* = \frac{t}{\tau}, \omega^*_{1,1} = \omega_{1,1}\tau, \ \Omega = \omega\tau, \ \eta_d = \frac{\eta}{\tau}, \tag{29}$$

where $D = \frac{1}{12\left(1-\nu^2\right)} Eh^3$ and $\tau = \sqrt{\rho a^4 h/D}$; the asterisk notation is dropped in the following for brevity. Additionally, The characteristic length-scale of the aluminium is obtained as l=1.0653 μm (for the thickness of h=3 μm) utilising the experimental data reported in Ref. [44] as well as the analytical formula suggested in Ref. [45].

The frequency-response diagram of an imperfect viscoelastic microplate is depicted in Fig. 2 with A_0=0.3, η_s=0.0004, and f_1=90.0; the dimensionless linear natural frequency of the imperfect viscoelastic microplate in the (1,1) mode is obtained as $\omega_{1,1}$ =51.3751. Subfigure (a) shows the maximum amplitude of the dimensionless transverse displacement ($w_{\max}$) at x=0.5 and y=0.5; accordingly, the maximum amplitude of the dimensionless in-plane displacement ($u_{\max}$) for x=0.66 and y=0.5 is shown in subfigure (b) – the v motion is the same as the u one, since the in-plane dimensions of the microplate are the same. As seen in this figure, the maximum amplitude of the in-plane motion is much smaller than that of the transverse motion. The figure shows that the peak of the resonant response is inclined toward the higher excitation frequency region, highlighting a hardening-type nonlinear behaviour. Moreover, as seen in both the subfigures, the response is heavily damped and the curves at the peak amplitudes are not sharp. Furthermore, for low excitation frequencies, the amplitude of the

response increases along the stable solution (indicated by a solid line). At a sufficiently high excitation frequency (i.e. at point A with $\Omega/\omega_{1,1}$= 1.0724), the response of the imperfect viscoelastic microplate jumps to a lower amplitude, abruptly. This jump phenomenon is arising from the existence of a saddle-node bifurcation in which the stable response turns to an unstable one. A similar scenario appears as the frequency of the excitation load decreases; the viscoelastic microsystem exhibits the second jump at point B where $\Omega/\omega_{1,1}$= 1.0204, indicating the existence of the second saddle-node bifurcation.

Figure 3 highlights the effect of the imperfection amplitude on the frequency-response curves of the imperfect viscoelastic microplate. In this figure, different values of the imperfection amplitude (A_0) is selected while the rest of the parameters are kept fixed (η_s=0.0004 and f_1=90.0). It can be observed in the figure that by increasing the imperfection amplitude, the nonlinear behaviour of the viscoelastic microsystem alters both qualitatively and quantitatively. The imperfect viscoelastic microplate undergoes four saddle-node bifurcations when A_0=0.4 giving rise to additional jumps in the response of the microsystem. Moreover, the maximum amplitude of the transverse motion is larger for the smaller values of the imperfection amplitude (i.e. A_0=0.2); however, the maximum amplitude of the longitudinal motion is not affected much by the amplitude of the imperfection. It should be noted that the general behaviour of the imperfect viscoelastic microplate tends to be softening/hardening from pure hardening when A_0 is increased. Moreover, a large value for A_0 results in a shift of the curve to the right.

Figure 4 highlights the importance of the nonlinear amplitude-dependent damping originating from the viscoelastic model by comparing the resonant response of the viscoelastic model with that of an elastic one. Note that by setting the Kelvin-Voigt viscosity coefficient η equal to zero, the viscoelastic model of the microplate reduces to the elastic model; a linear viscous damping term is then added to the governing equations – a modal damping ratio of ζ= 0.0102 is utilised in the numerical simulations. The frequency-response curves are plotted for an imperfect microplate with A_0=0.3, subjected to different values of the forcing amplitude. In order to obtain similar predictions based on the two models, a dimensionless damping coefficient of ζ =0.0102 is considered for the linear viscous damping; η_s is set to 0.0004 for the imperfect viscoelastic microplate. As seen in the figure, for the small value of the excitation amplitude (i.e. f_1=10), both models end up showing an identical nonlinear behaviour. As the forcing amplitude is set to larger values, the elastic model (which possesses a linear viscous damping mechanism) predicts larger maximum amplitudes of motion in both the transverse and in-plane directions compared to the nonlinear viscoelastic model. In fact, the effect of the nonlinear damping term becomes more dominant for larger external forces. The discrepancy becomes more noticeable for f_1=80, where the peak amplitudes deviate from each other substantially. This highlights the impact of the research reported in this paper.

In order to better highlight the contribution of the amplitude-dependent nonlinear damping terms in the viscoelastic model, Fig. 5 is plotted which shows the forcing amplitude versus the nonlinear excitation frequency of the peak resonant amplitudes of the imperfect viscoelastic microplate with A_0=0.3. As already mentioned, the gap between the two models is negligible for small oscillation amplitudes (i.e. f_1<25); for larger values of the forcing amplitude,

however, the elastic model with linear viscous damping gives larger values for the nonlinear resonance frequencies compared to those predicted by the viscoelastic nonlinear model.

Similar numerical simulations are conducted on the same imperfect viscoelastic microplate and the results are plotted in Figs. 6 and 7; the only difference of the system of Figs. 6 and 7 to that of Figs. 4 and 5 is that the amplitude of imperfection is increased to A_0=0.4. Figure 6 shows the difference between the frequency-response curves of the elastic model with the linear viscous damping and the viscoelastic model with nonlinear damping mechanism; the results show the same trend as discussed earlier. Interestingly, for larger values of the excitation amplitude (i.e. f_1=60), a complex response with additional peaks is observed for the case of elastic model with linear viscous term (compare with Fig. 4, where there are no extra peaks). These extra peaks correspond to internal resonances [46] between the modes of vibration due to the presence of fairly large amplitude of the geometric imperfection. Indeed, increasing the amplitude of the imperfection results in a shift in the dimensionless linear natural frequency of the imperfect viscoelastic microplate and leads the microsystem to undergo an internal resonance. The amplitude of the extra peaks and the presence of the additional branches in the solution are more noticeable for f_1=100. However, these additional peaks diminish for the case of the viscoelastic model where the nonlinear amplitude-dependent damping term is involved.

Figure 8 highlights the differences in the predicted response of an imperfect viscoelastic microplate modelled on the basis of the classical continuum theory and MCST frameworks; for both the models, A_0=0.3, η_s=0.0004, and f_1=90.0 are selected. It should be noted that the MCST

reduces to the classical continuum theory when the length-scale parameter is equal to zero. As seen in this figure, taking into account the size-dependent behaviour of the microsystem in the model can alter the response dramatically. More specifically, the fundamental natural frequency of the imperfect viscoelastic microplate is obtained as $\omega_{1,1} = 51.3751$ based on MCST while it is predicted as $\omega_{1,1} = 44.5010$ based on the classical continuum theory. Consequently, the classical continuum theory predicts the nonlinear resonance frequency at lower excitation frequencies compared to that of MCST. Moreover, the maximum amplitude of the motions (both transverse and longitudinal) are slightly smaller for the case of the classical continuum theory; this is contradictory to the initial expectation that since the length-scale parameter stiffens the system the vibration amplitude should be smaller, however, when both the nonlinear viscoelasticity and small-size effects are present together, the peak oscillation amplitude based on MCST is larger than that based on the classical continuum.

Figure 9 shows a parametric analysis on the effect of the length-scale on the nonlinear resonant response of the imperfect viscoelastic microplate. As seen in the figure, as a result of increased value of length-scale, the nonlinear resonance region occurs at larger excitation frequencies, which is an indication of increased linear natural frequency as well. Furthermore, it is observed that the maximum transverse displacement increases due to increased length-scale parameter. Figure 9 also reveals that at larger values of the length-scale parameter, the microsystem displays a weaker nonlinear behaviour.

4. Conclusions

A viscoelastically coupled nonlinear model for an imperfect microplate has been developed in this paper. The Kirchhoff plate theory together with MCST accounting for size-dependent behaviour of the microsystem and the Kelvin–Voigt model accounting for the nonlinear amplitude-dependent damping of the microsystem were employed. The nonlinear partial differential equations of motion were obtained using Hamilton's framework and discretised with the aid of the Galerkin scheme. The resonant response of the imperfect viscoelastic microsystem was examined through extensive numerical simulations via plotting the frequency-response curves utilising a continuation scheme together with time-integration. The simulation results highlighted that:

- The general behaviour of the viscoelastic imperfect microplate is a hardening-type response with two or more saddle-node bifurcations.
- At relatively small forcing amplitudes, both elastic model with linear damping as well as the viscoelastic model predict very similar response.
- At sufficiently large forcing amplitudes, the contribution of the nonlinear amplitude-dependent damping terms becomes more dominant.
- Increasing the amplitude of the imperfection gives rise to a change in the general behaviour of the imperfect viscoelastic microplate.
- Increasing the length-scale parameter results in increased transverse amplitude of oscillation and weakened nonlinear behaviour as well as increased resonant frequency of oscillation.

References

[1] C. Rembe, R.S. Muller, Measurement system for full three-dimensional motion characterization of MEMS, Journal of Microelectromechanical Systems, 11 (2002) 479-488.

[2] R.P. LaRose Iii, K.D. Murphy, Impact dynamics of MEMS switches, Nonlinear Dynamics, 60 (2010) 327-339.

[3] D.I. Caruntu, I. Martinez, M.W. Knecht, Reduced order model analysis of frequency response of alternating current near half natural frequency electrostatically actuated MEMS cantilevers, Journal of Computational and Nonlinear Dynamics, 8 (2013).

[4] P. Belardinelli, S. Lenci, M. Brocchini, Modeling and analysis of an electrically actuated microbeam based on nonclassical beam theory, ASME Journal of Computational and Nonlinear Dynamics, 9 (2014) 031016-031016.

[5] H. Madinei, G. Rezazadeh, S. Azizi, Stability and bifurcation analysis of an asymmetrically electrostatically actuated microbeam, ASME Journal of Computational and Nonlinear Dynamics, 10 (2015) 021002-021002.

[6] L. Ruzziconi, M.I. Younis, S. Lenci, An efficient reduced-order model to investigate the behavior of an imperfect microbeam under axial load and electric excitation, Journal of Computational and Nonlinear Dynamics, 8 (2013).

[7] J. Awrejcewicz, A.V. Krysko, S.P. Pavlov, M.V. Zhigalov, V.A. Krysko, Chaotic dynamics of size dependent Timoshenko beams with functionally graded properties along their thickness, Mechanical Systems and Signal Processing, 93 (2017) 415-430.

[8] A.J. Dick, B. Balachandran, C.D. Mote Jr, Localization in microresonator arrays: Influence of natural frequency tuning, Journal of Computational and Nonlinear Dynamics, 5 (2010) 1-11.

[9] M.H. Ghayesh, H. Farokhi, M. Amabili, Nonlinear behaviour of electrically actuated MEMS resonators, International Journal of Engineering Science, 71 (2013) 137-155.

[10] M.H. Ghayesh, H. Farokhi, G. Alici, Size-dependent performance of microgyroscopes, International Journal of Engineering Science, 100 (2016) 99-111.

[11] N.A. Fleck, G.M. Muller, M.F. Ashby, J.W. Hutchinson, Strain gradient plasticity: Theory and experiment, Acta Metallurgica et Materialia, 42 (1994) 475-487.

[12] A.W. McFarland, J.S. Colton, Role of material microstructure in plate stiffness with relevance to microcantilever sensors, Journal of Micromechanics and Microengineering, 15 (2005) 1060.

[13] M.H. Ghayesh, H. Farokhi, Chaotic motion of a parametrically excited microbeam, International Journal of Engineering Science, 96 (2015) 34-45.

[14] M.H. Ghayesh, M. Amabili, H. Farokhi, Three-dimensional nonlinear size-dependent behaviour of Timoshenko microbeams, International Journal of Engineering Science, 71 (2013) 1-14.

[15] H. Farokhi, M.H. Ghayesh, M. Amabili, Nonlinear dynamics of a geometrically imperfect microbeam based on the modified couple stress theory, International Journal of Engineering Science, 68 (2013) 11-23.

[16] M.H. Ghayesh, H. Farokhi, M. Amabili, Nonlinear dynamics of a microscale beam based on the modified couple stress theory, Composites Part B: Engineering, 50 (2013) 318-324.

[17] R.S. Lakes, Viscoelastic materials, Cambridge University Press, 2009.

[18] S. Zaitsev, O. Shtempluck, E. Buks, O. Gottlieb, Nonlinear damping in a micromechanical oscillator, Nonlinear Dynamics, 67 (2012) 859-883.

[19] W. Zhang, Y. Huang, M. Yao, Multi-pulse homoclinic orbits and chaotic dynamics of a parametrically excited nonlinear nano-oscillator with coupled cubic nonlinearities, Science China Physics, Mechanics & Astronomy, 57 (2014) 1098-1110.

[20] W. Zhang, Y. Hao, J. Yang, Nonlinear dynamics of FGM circular cylindrical shell with clamped–clamped edges, Composite Structures, 94 (2012) 1075-1086.

[21] Y. Hao, W. Zhang, J. Yang, Nonlinear oscillation of a cantilever FGM rectangular plate based on third-order plate theory and asymptotic perturbation method, Composites Part B: Engineering, 42 (2011) 402-413.

[22] W. Zhang, J. Yang, Y. Hao, Chaotic vibrations of an orthotropic FGM rectangular plate based on third-order shear deformation theory, Nonlinear Dynamics, 59 (2010) 619-660.

[23] Y. Hao, L. Chen, W. Zhang, J. Lei, Nonlinear oscillations, bifurcations and chaos of functionally graded materials plate, Journal of Sound and Vibration, 312 (2008) 862-892.

[24] S. Mahmoodi, S.E. Khadem, M. Kokabi, Non-linear free vibrations of Kelvin–Voigt visco-elastic beams, International Journal of Mechanical Sciences, 49 (2007) 722-732.

[25] Y. Lei, S. Adhikari, M. Friswell, Vibration of nonlocal Kelvin–Voigt viscoelastic damped Timoshenko beams, International Journal of Engineering Science, 66 (2013) 1-13.

[26] M. Namvar, E. Rezaei, S.A. Hosseini, M. Ghadiri, Experimental and analytical investigations of vibrational behavior of U-shaped atomic force microscope probe considering thermal loading and the modified couple stress theory, The European Physical Journal Plus, 132 (2017) 247.

[27] O. Rahmani, S. Hosseini, I. Ghoytasi, H. Golmohammadi, Free vibration of deep curved FG nano-beam based on modified couple stress theory, Steel and Composite Structures, 26 (2018) 607-620.

[28] R. Sourki, S. Hosseini, Coupling effects of nonlocal and modified couple stress theories incorporating surface energy on analytical transverse vibration of a weakened nanobeam, The European Physical Journal Plus, 132 (2017) 184.

[29] M. Zarepour, S.A. Hosseini, A semi analytical method for electro-thermo-mechanical nonlinear vibration analysis of nanobeam resting on the Winkler-Pasternak foundations with general elastic boundary conditions, Smart Materials and Structures, 25 (2016) 085005.

[30] S.H. Hashemi, A.T. Samaei, Buckling analysis of micro/nanoscale plates via nonlocal elasticity theory, Physica E: Low-dimensional Systems and Nanostructures, 43 (2011) 1400-1404.

[31] E. Jomehzadeh, H.R. Noori, A.R. Saidi, The size-dependent vibration analysis of micro-plates based on a modified couple stress theory, Physica E: Low-dimensional Systems and Nanostructures, 43 (2011) 877-883.

[32] B. Wang, S. Zhou, J. Zhao, X. Chen, A size-dependent Kirchhoff micro-plate model based on strain gradient elasticity theory, European Journal of Mechanics - A/Solids, 30 (2011) 517-524.

[33] C.M.C. Roque, A.J.M. Ferreira, J.N. Reddy, Analysis of Mindlin micro plates with a modified couple stress theory and a meshless method, Applied Mathematical Modelling, 37 (2013) 4626-4633.

[34] A. Nabian, G. Rezazadeh, M. Almassi, A.-M. Borgheei, On the stability of a functionally graded rectangular micro-plate subjected to hydrostatic and nonlinear electrostatic pressures, Acta Mechanica Solida Sinica, 26 (2013) 205-220.

[35] A. Ashoori Movassagh, M.J. Mahmoodi, A micro-scale modeling of Kirchhoff plate based on modified strain-gradient elasticity theory, European Journal of Mechanics - A/Solids, 40 (2013) 50-59.

[36] A. Farajpour, A.R. Shahidi, M. Mohammadi, M. Mahzoon, Buckling of orthotropic micro/nanoscale plates under linearly varying in-plane load via nonlocal continuum mechanics, Composite Structures, 94 (2012) 1605-1615.

[37] P. Belardinelli, S. Lenci, L. Demeio, A comparison of different semi-analytical techniques to determine the nonlinear oscillations of a slender microbeam, Meccanica, 49 (2014) 1821-1831.

[38] M. Asghari, Geometrically nonlinear micro-plate formulation based on the modified couple stress theory, International Journal of Engineering Science, 51 (2012) 292-309.

[39] H.-T. Thai, D.-H. Choi, Size-dependent functionally graded Kirchhoff and Mindlin plate models based on a modified couple stress theory, Composite Structures, 95 (2013) 142-153.

[40] A. Gholipour, H. Farokhi, M.H. Ghayesh, In-plane and out-of-plane nonlinear size-dependent dynamics of microplates, Nonlinear Dynamics, 79 (2015) 1771-1785.

[41] M.H. Ghayesh, H. Farokhi, Nonlinear dynamics of microplates, International Journal of Engineering Science, 86 (2015) 60-73.

[42] F. Yang, A.C.M. Chong, D.C.C. Lam, P. Tong, Couple stress based strain gradient theory for elasticity, International Journal of Solids and Structures, 39 (2002) 2731-2743.

[43] H. Farokhi, M.H. Ghayesh, Thermo-mechanical dynamics of perfect and imperfect Timoshenko microbeams, International Journal of Engineering Science, 91 (2015) 12-33.

[44] M.A. Haque, M.T.A. Saif, Strain gradient effect in nanoscale thin films, Acta Materialia, 51 (2003) 3053-3061.

[45] S.H. Chen, B. Feng, Size effect in micro-scale cantilever beam bending, Acta Mechanica, 219 (2011) 291-307.

[46] M.H. Ghayesh, H. Farokhi, M. Amabili, In-plane and out-of-plane motion characteristics of microbeams with modal interactions, Composites Part B: Engineering, 60 (2014) 423-439.

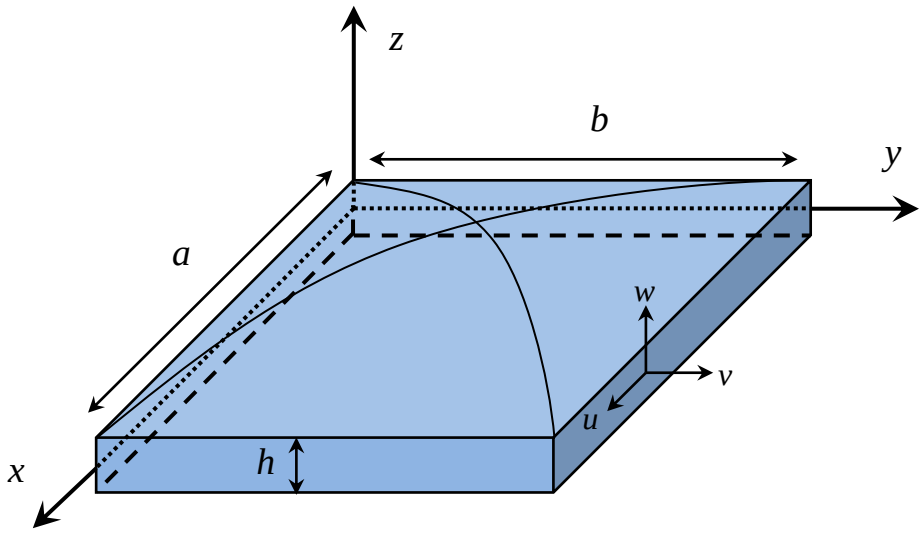

Figure 1: Schematic of an imperfect microscale plate.

(a)

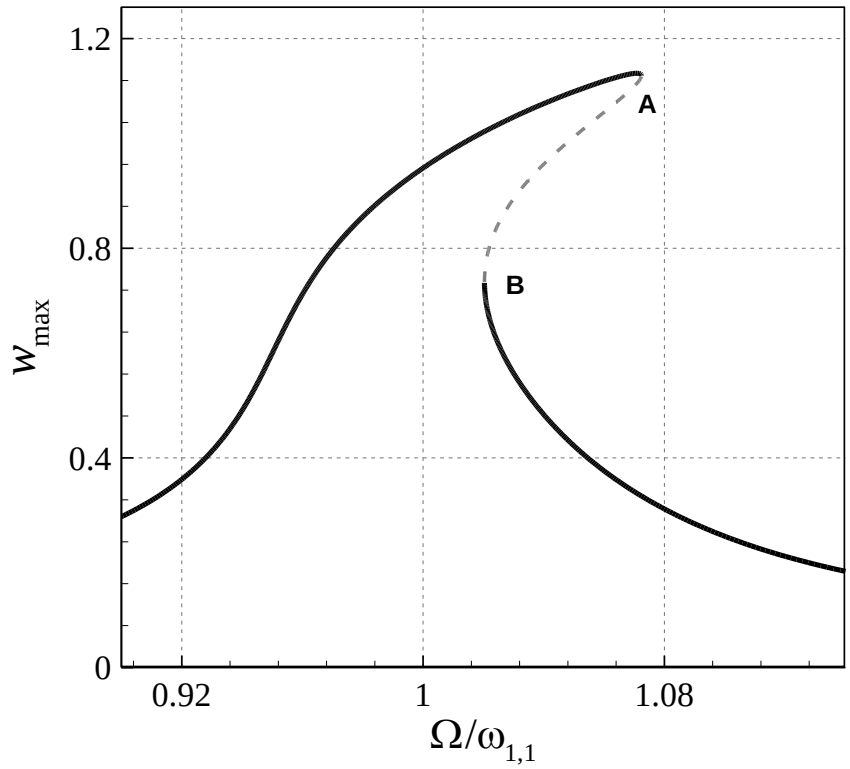

(b)

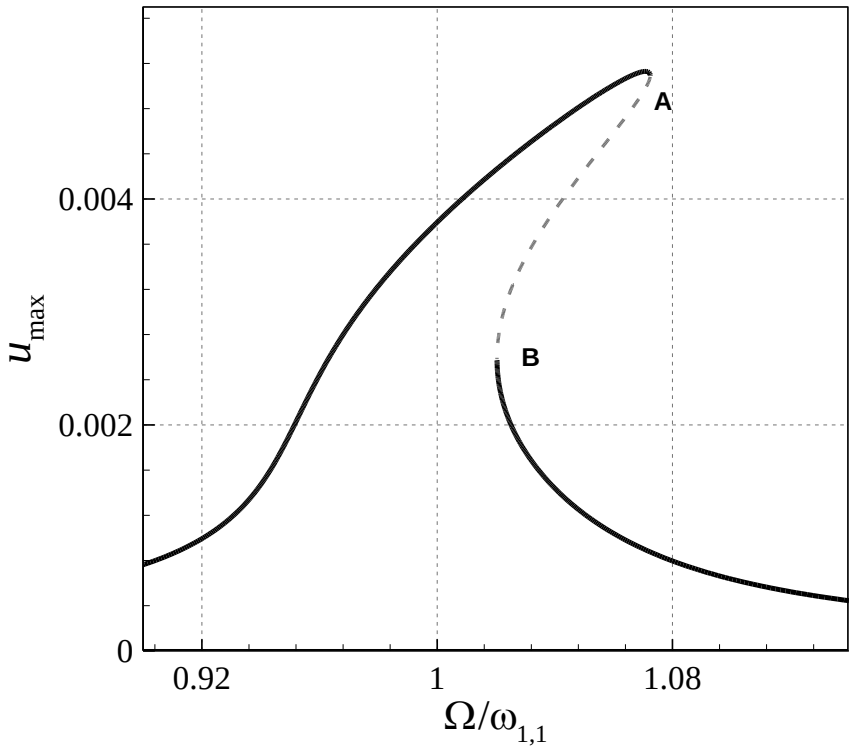

Figure 2: Frequency-amplitude plots of the initially imperfect viscoelastic microplate: (a) the maximum transverse displacement at microplate centre (x=0.5 and y=0.5); (b) the maximum longitudinal displacement (x=0.66 and y=0.5); A_0=0.3, f_1=90.0, and η_s=0.0004. Solid line: stable solution; dashed line: unstable solution.

(a)

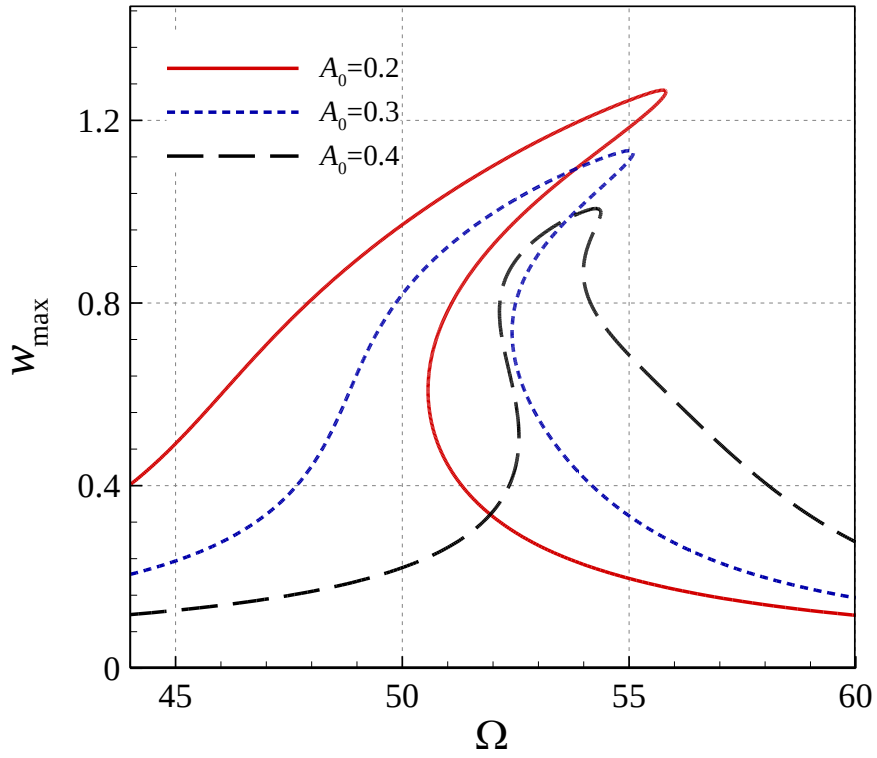

(b)

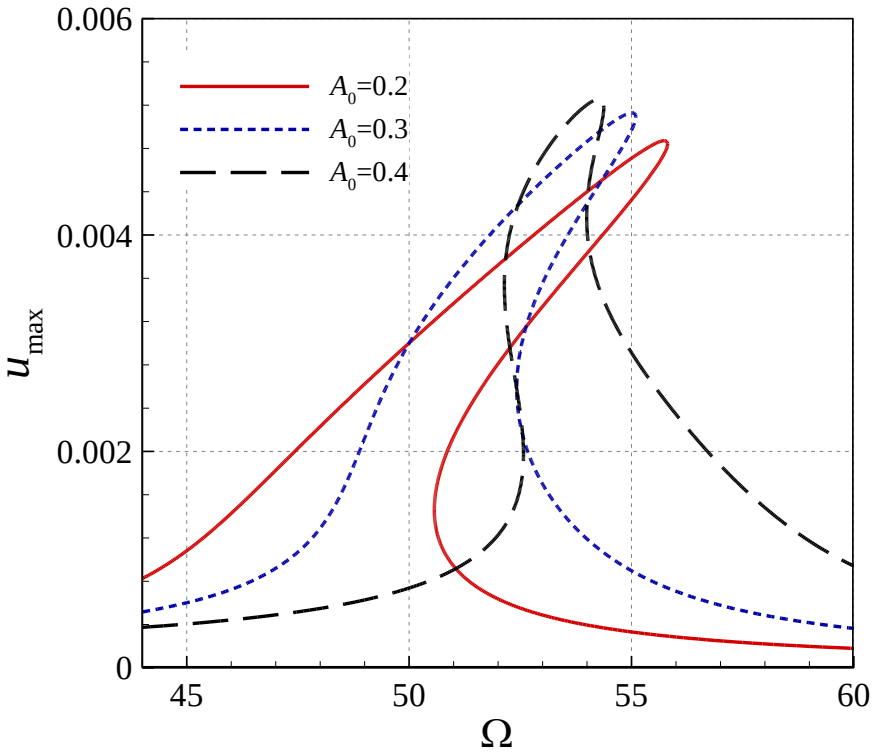

Figure 3: Frequency-amplitude plots of the viscoelastic microplate for different imperfection amplitudes: (a) the maximum transverse displacement at microplate centre (x=0.5 and y=0.5); (b) the maximum longitudinal displacement (x=0.66 and y=0.5); f_1=90.0 and η_s=0.0004.

(a)

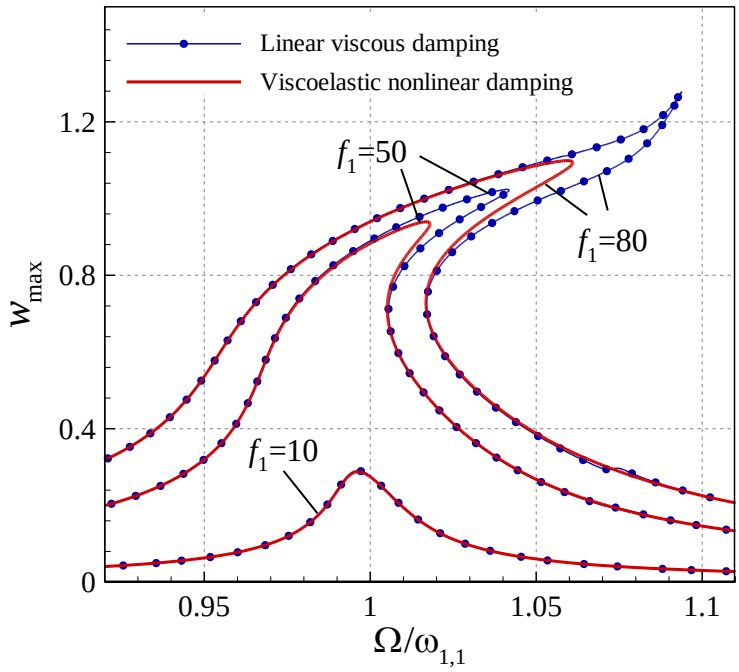

(b)

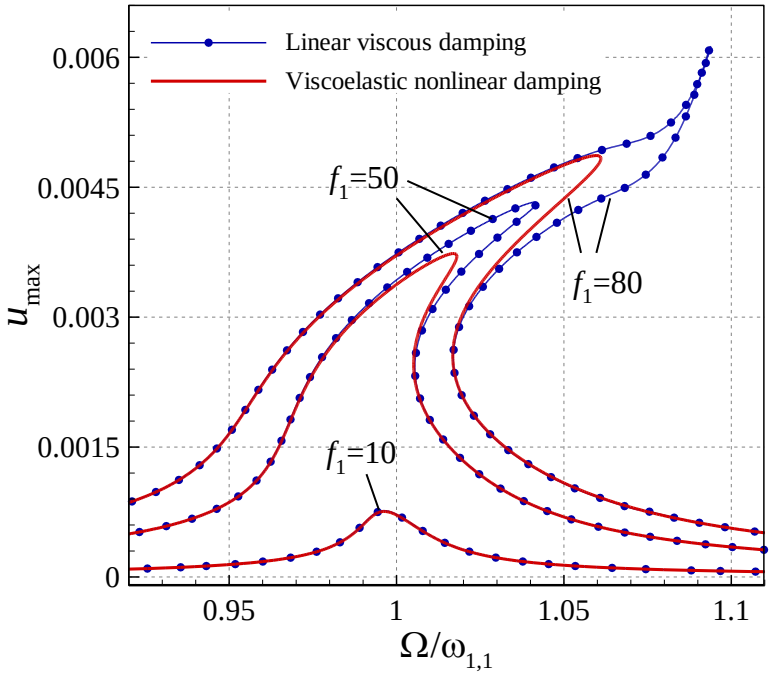

Figure 4: Frequency-amplitude plots of the linear viscous damping (ζ= 0.0102) and viscoelastic nonlinear damping (η_s=0.0004) models of the imperfect microsystem for different forcing amplitudes: (a) the maximum transverse displacement at microplate centre (x=0.5 and y=0.5); (b) the maximum longitudinal displacement (x=0.66 and y=0.5); A_0=0.3.

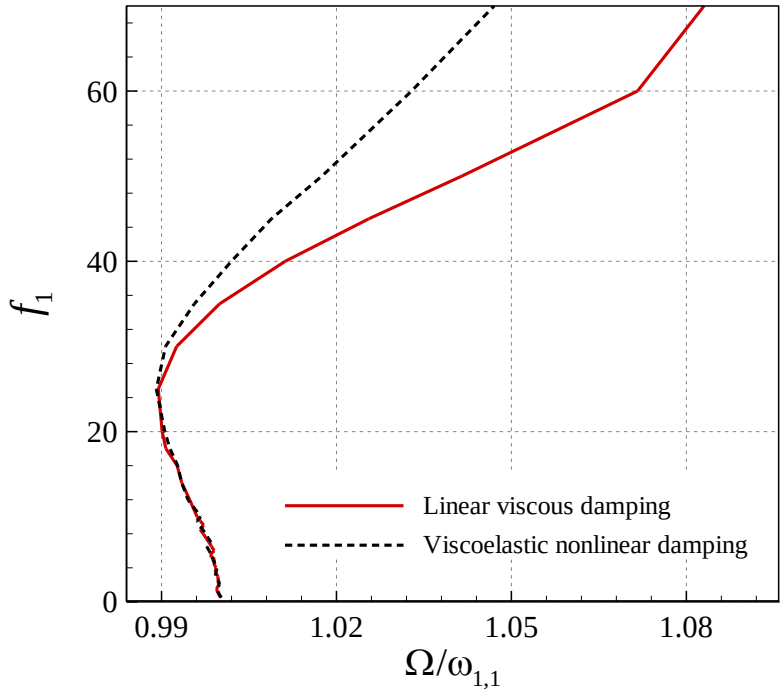

Figure 5: Excitation frequency at nonlinear resonance versus the amplitude of the dynamic load for linear viscous damping (ζ= 0.0102) and viscoelastic nonlinear damping (η_s=0.0004) models of the imperfect microsystem; A_0=0.3.

(a)

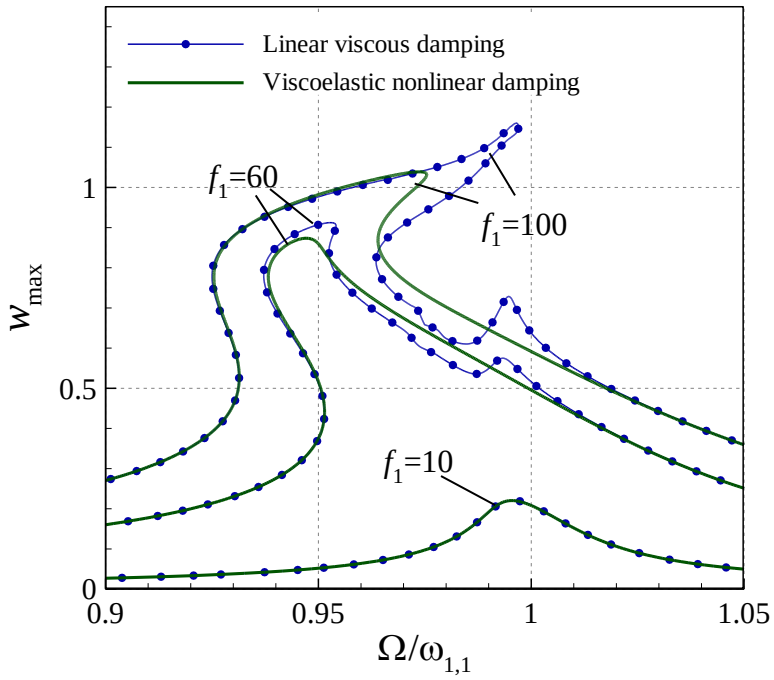

(b)

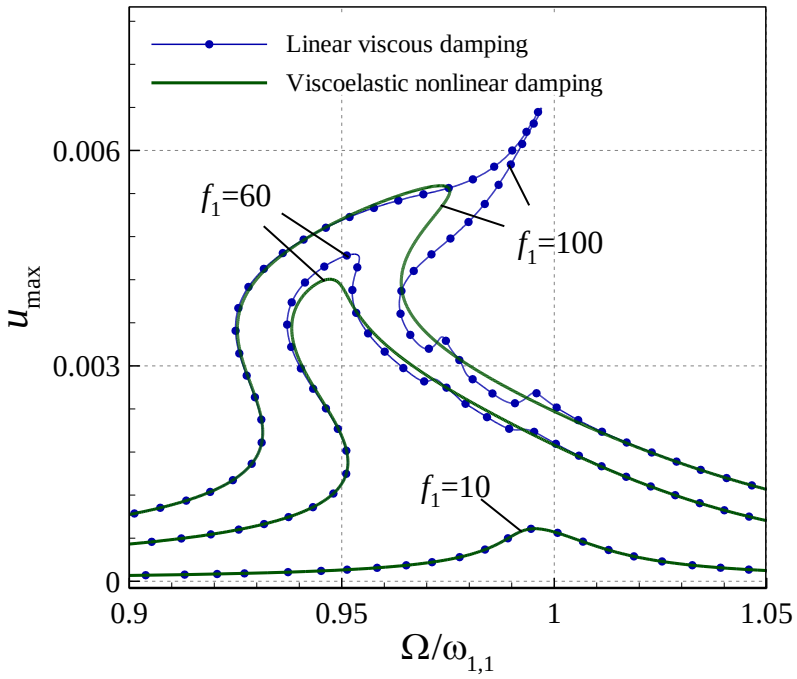

Figure 6: Frequency-amplitude plots of the linear viscous damping (ζ= 0.0102) and viscoelastic nonlinear damping (η_s=0.0004) models of the imperfect microsystem for different forcing amplitudes: (a) the maximum transverse displacement at microplate centre (x=0.5 and y=0.5); (b) the maximum longitudinal displacement (x=0.66 and y=0.5); A_0=0.4.

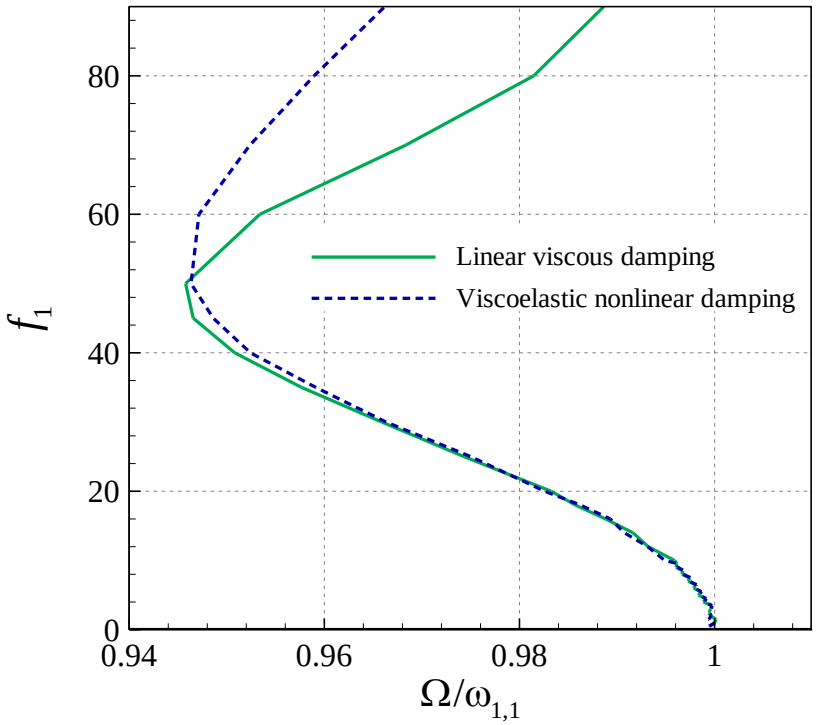

Figure 7: Excitation frequency at nonlinear resonance versus the amplitude of the dynamic load for linear viscous damping (ζ= 0.0102) and viscoelastic nonlinear damping (η_s=0.0004) models of the imperfect microsystem; A_0=0.4.

(a)

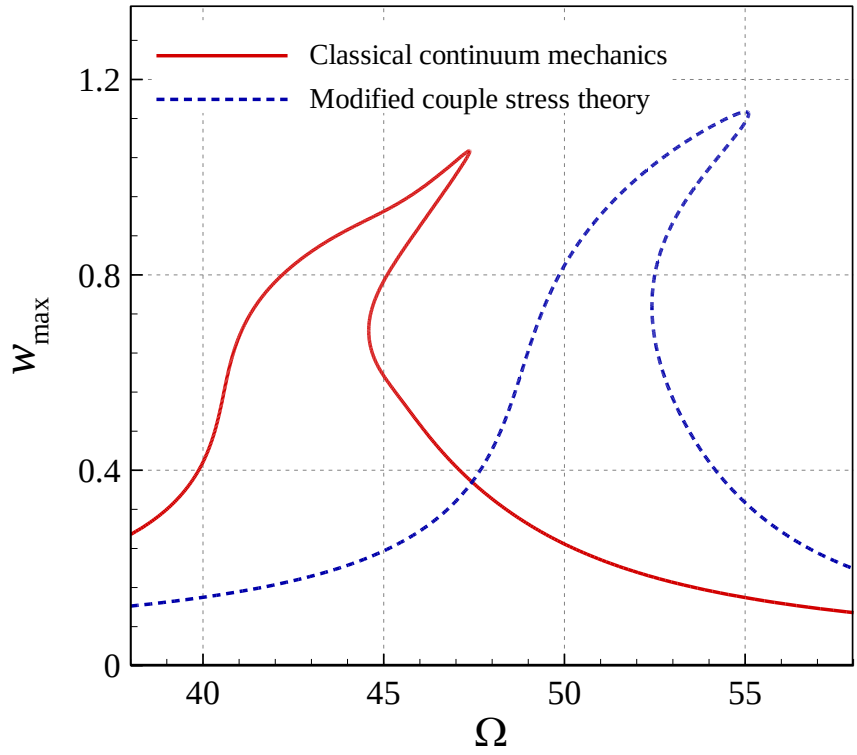

(b)

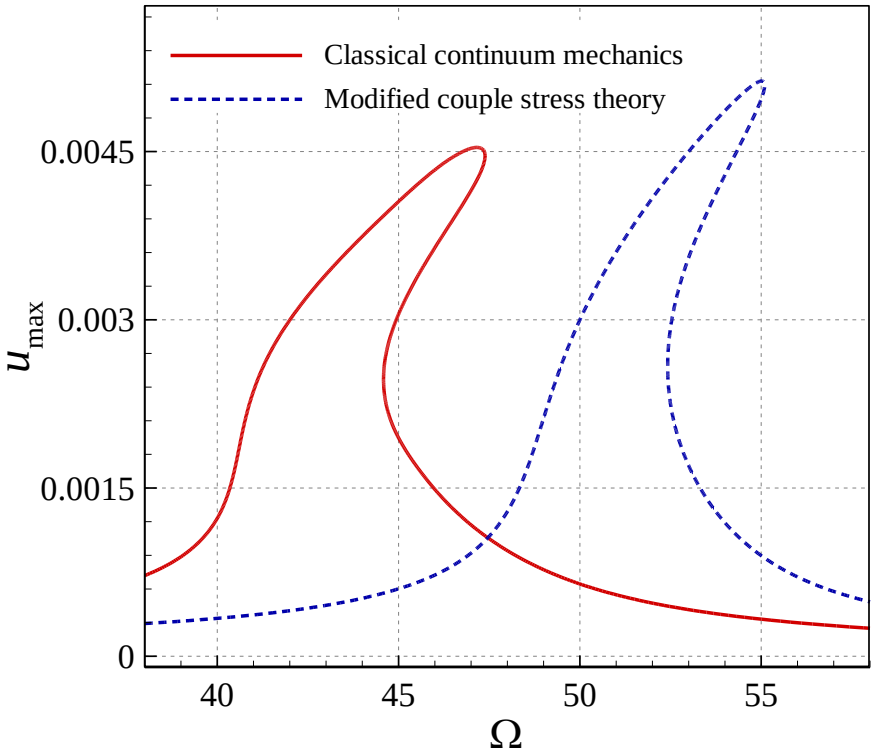

Figure 8: Frequency-amplitude plots of the viscoelastic microplate for modified couple stress theory ($\omega_{1,1}$ =51.3751) and classical continuum mechanics ($\omega_{1,1}$ =44.5010): (a) the maximum transverse displacement at microplate centre (x=0.5 and y=0.5); (b) the maximum longitudinal displacement (x=0.66 and y=0.5); A_0=0.3, f_1=90.0, and η_s=0.0004.

(a)

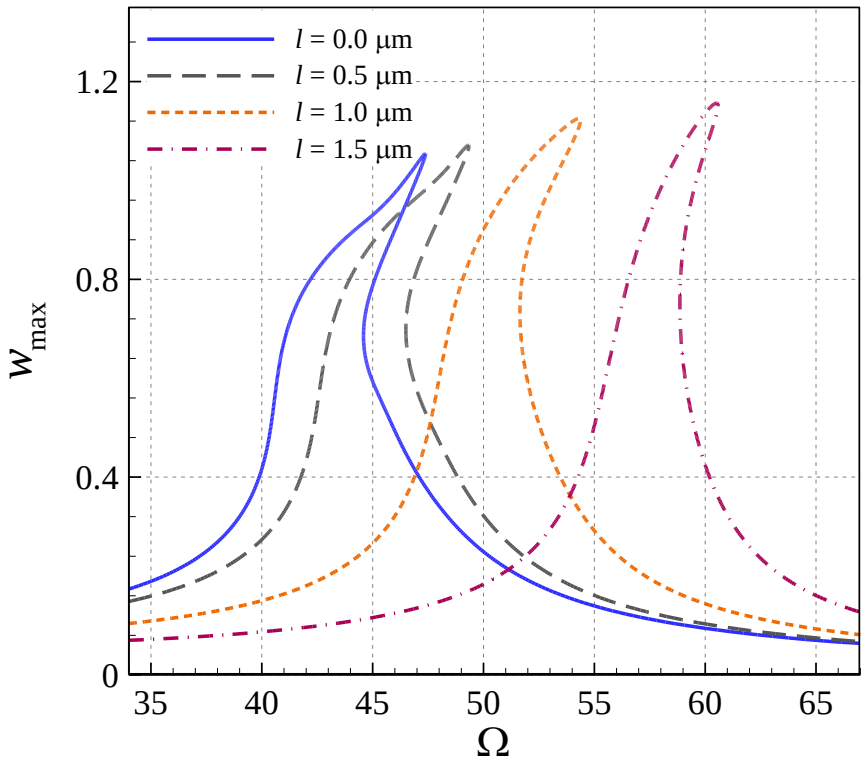

(b)

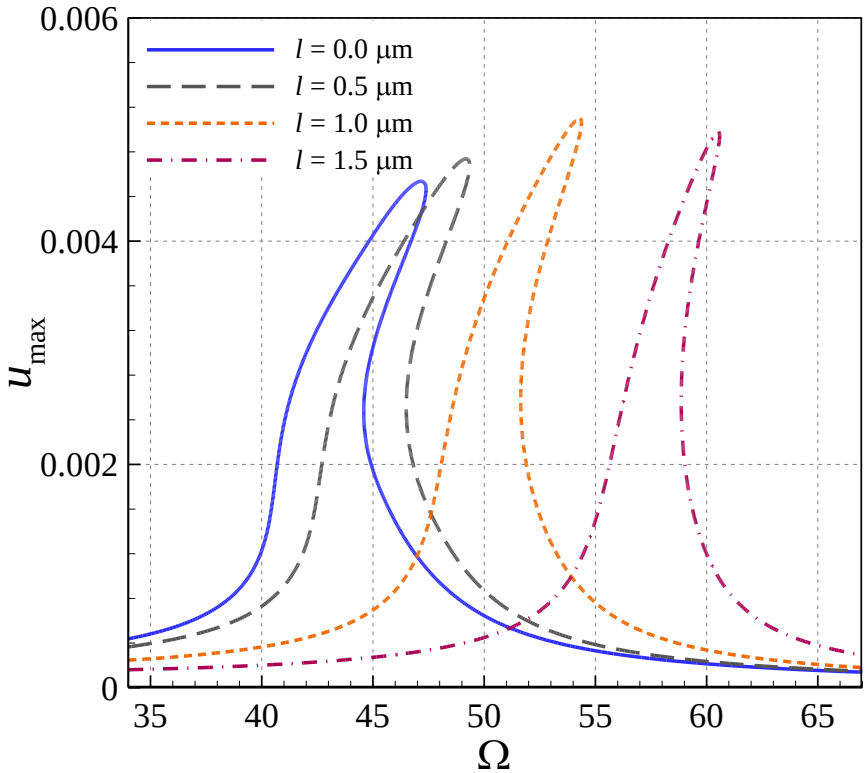

Figure 9: Small scale effects on the frequency-amplitude plots of the viscoelastic microplate: (a) the maximum transverse displacement at microplate centre (x=0.5 and y=0.5); (b) the maximum longitudinal displacement (x=0.66 and y=0.5); A_0=0.3, f_1=90.0, and η_s=0.0004.